**Healy-Kalesh, MW, Sasaki, M, Points, SD, Filipović, MD, Smeaton, ZJ, Darnley, MJ, Long, KS, Saeedi, S and Zangrandi, F**

**Discovery of a nova super-remnant surrounding the recurrent nova LMCN 1971-08a in the Large Magellanic Cloud**

A&A, 702, L9 (2025)
https://doi.org/10.1051/0004-6361/202556670


Astronomy & Astrophysics

LETTER TO THE EDITOR

# Discovery of a nova super-remnant surrounding the recurrent nova LMCN 1971-08a in the Large Magellanic Cloud

Michael W. Healy-Kalesh[1,2,⋆,⋆⋆], Manami Sasaki[1], Sean D. Points[3], Miroslav D. Filipović[4], Zachary J. Smeaton[4], Matthew J. Darnley[2], Knox S. Long[5,6], Sara Saeedi[1], and Federico Zangrandi[1]

[1] Dr. Karl Remeis Observatory, Erlangen Centre for Astroparticle Physics, Friedrich-Alexander-Universität Erlangen-Nürnberg, Sternwartstraße 7, 96049 Bamberg, Germany
[2] Astrophysics Research Institute, Liverpool John Moores University, Liverpool L3 5RF, UK
[3] NSF's NOIRLab/CTIO, Casilla 603, La Serena 1700000, Chile
[4] School of Science, Western Sydney University, Locked Bag 1797, Penrith, NSW 2751, Australia
[5] Space Telescope Science Institute, 3700 San Martin Drive, Baltimore, MD 21218, USA
[6] Eureka Scientific, Inc., 2452 Delmer Street, Suite 100, Oakland, CA 94602-3017, USA

Received 30 July 2025 / Accepted 16 September 2025

**ABSTRACT**

A nova super-remnant (NSR) is a greatly-extended structure grown by repeated nova eruptions sweeping the surrounding material away from a nova into a dense outer shell and are predicted to form around all novae. To date, four NSRs are known, with three located in the Galaxy and one residing in M31. Here we present the discovery of the first NSR in the Large Magellanic Cloud and only the second extragalactic nova shell identified, hosted by the recurrent nova LMCN 1971-08a. The structure is coincident with the nova, has a circular morphology, and is visible in narrowband H$\alpha$ and [S II] filters but is very faint in [O III], as expected. H I data also potentially reveal the existence of a coincident structure. Further, with a diameter of ~200 pc, this NSR is the largest example yet found, with models indicating an ~4130 $M_\odot$ shell expanding at ~20 km s$^{-1}$ into the surrounding medium and an age of ~2.4 Myr. The existence of the NSR also suggests that LMCN 1971-08a may have a much shorter recurrence period than currently presumed.

**Key words.** novae, cataclysmic variables – stars: individual: LMCN 1971-08a – ISM: structure – Magellanic Clouds – radio continuum: ISM

## 1. Introduction

Recurrent novae (RNe) are observationally-defined as accreting white dwarf (WD) binaries that have exhibited more than one nova eruption. Such eruptions are driven by a thermonuclear runaway on the WD's surface (Starrfield et al. 1972), which leads to a portion of the accreted material being ejected at velocities up to thousands of kilometers per second (O'Brien et al. 2001); in some cases, this material forms expanding subparsec nova shells (Shara et al. 2024a; Santamaría et al. 2025). After the eruption, the resumption of accretion onto the WD (Worters et al. 2007) prepares the nova system for subsequent eruptions. Furthermore, accumulation of material retained on the WD following each eruption can grow the WD (Yaron et al. 2005; Hillman et al. 2016) to the Chandrasekhar limit to potentially explode as a type Ia supernova (Whelan & Iben 1973).

Nova super-remnants (NSRs) are shell-like structures orders of magnitude larger than singular eruption nova shells (for a review see Healy-Kalesh 2024). The first NSR (Darnley et al. 2019) was discovered in the Andromeda Galaxy around the rapidly recurring nova, M31N 2008-12a and formed by the ejecta of repeated nova eruptions over millennia, excavating tens of thousands of solar masses of surrounding interstellar medium from around the central binary into a high-density shell (Darnley et al. 2019). Theoretically, such structures should encompass all novae (Healy-Kalesh et al. 2023), although their size on the sky and low surface brightnesses make NSRs difficult to find in optical data. However, with the capabilities of the recently deployed Condor Array Telescope (Lanzetta et al. 2023), optical NSRs have now been discovered around the Galactic RNe KT Eridani (Shara et al. 2024b; Healy-Kalesh et al. 2024a), T Coronae Borealis (Shara et al. 2024c) and RS Ophiuchi (Shara et al. 2025)[1]. These NSRs have diameters ranging from ~30−130 pc; have emission most prominent in H$\alpha$, [S II] and [N II]; lack strong [O III] emission as a result of ionisation from low velocity shocks; and exhibit low expansion velocities in their outer shells. While the NSR around M31N 2008-12a appears to have a more well-defined elliptical shell as it is viewed pole-on (Darnley et al. 2019), the Galactic NSRs have more patchy morphologies likely as a result of the NSR growing within the irregular interstellar medium (ISM) and possibly from being observed at different viewing angles. Furthermore, the NSRs surrounding T CrB (Shara et al. 2024c) and RS Oph (Shara et al. 2025) appear bilobed, possibly resulting from the ejecta being initially influenced by the accretion disk around the WD. A search for additional NSRs in M31 and the Large Magellanic Cloud (LMC) did not yield further

⋆ Corresponding author: michael.healy-kalesh@fau.de, M.W.HealyKalesh@ljmu.ac.uk
⋆⋆ Honorary Visiting Research Fellow at Liverpool John Moores University.

[1] A possible cavity component of the NSR associated with RS Ophiuchi was identified in far-infrared data (Healy-Kalesh et al. 2024c).

examples (Healy-Kalesh et al. 2024b), but this apparent dearth was attributed to the structures around other "younger" systems being considerably fainter.

LMCN 1971-08a is one of the four currently known recurrent novae in the LMC. It exhibited eruptions in 1971 (Graham 1971) and 2009 (Liller 2009) and therefore has a recurrence period (or inter-eruption interval) of ∼38/N years (Bode et al. 2016), where N may be one or a small integer. While only a spectrum of the first eruption was obtained in 1971 with no further follow-up (Graham 1971; Bode et al. 2016), the more recent eruption in 2009 was followed in great detail, being observed in the optical, UV, near-infrared (Bode et al. 2016), and X-rays (Bode et al. 2016; Orio et al. 2021). These observations revealed a very fast-declining nova comprising a 1.1−1.3 $M_\odot$ WD, accreting material at an elevated rate of $3.6^{+4.7}_{-2.5} \times 10^{-7}$ $M_\odot$ yr$^{-1}$ from a subgiant companion with a probable orbital period of 1.2 days (Bode et al. 2016). The ejecta velocities seen from the nova ranged from 1000−4200 km s$^{-1}$ (Orio et al. 2009; Bode et al. 2016) with shocks likely present in the ejecta before day nine of the eruption (Bode et al. 2016).

In this Letter, we present the discovery of a nova super-remnant around the recurrent nova LMCN 1971-08a, the first nova super-remnant to be found in the LMC. In Sect. 2 we outline the datasets used in this work before describing the characteristics of the NSR across optical and radio data in Sect. 3. In Sect. 4 we place the discovery within the context of the growing field of nova super-remnants and rule out other possible origins before summarising our findings in Sect. 5.

## 2. Optical and radio data

Within this study, several datasets were utilised across the optical and radio. The Magellanic Cloud Emission Line Survey (MCELS; Smith & Team 1999) observed the central 8° × 8° of the LMC with five filters including narrowband H$\alpha$, [S II] and [O III] filters. The DeMCELS survey (Points et al. 2024) is a contemporary higher-resolution emission-line survey of the Magellanic Clouds undertaken with the Dark Energy Camera (DECam; Flaugher et al. 2015) narrowband H$\alpha$ and [S II] filters. The continuum-subtracted narrowband data from both MCELS and DeMCELS were utilised for this work. The HI4PI survey (HI4PI Collaboration 2016) is an all-sky neutral atomic hydrogen (H I) survey constructed from the Effelsberg-Bonn H I Survey (EBHIS; Kerp et al. 2011) and the Galactic All-Sky Survey (GASS; McClure-Griffiths et al. 2009) data sets, which provide better angular resolution and sensitivity than previous all-sky H I surveys. The MeerKAT radio data (Cotton et al., in preparation) used in this work are from the MeerKAT array (Jonas & MeerKAT Team 2016), a new generation radio telescope with high resolution and sensitivity such that it is capable of resolving structures in the LMC (see, e.g., Sasaki et al. 2025).

## 3. LMCN 1971-08a nova super-remnant

A coherent, circular shell-like structure spatially coincident with LMCN 1971-08a appears in the MCELS H$\alpha$ data (see Fig. 1), with the same shell visible in the MCELS [S II] image but negligible in MCELS [O III], as expected for NSRs (Darnley et al. 2019; Shara et al. 2024b,c, 2025). While clearly evident in the MCELS data, the high resolution DeMCELS H$\alpha$ and [S II] imaging of the NSR emphasizes the structure further, as shown in Fig. B.1 (with the approximate extent of the NSR indicated).

With a distance of 49.6 ± 0.6 kpc to the LMC (Pietrzyński et al. 2019), the NSR has a projected diameter of ∼200 pc. As seen in the optical data of Fig. 1, the NSR is brighter to the northeast and southwest, with a fainter boundary connecting these two components to the northwest, defining the outer shell edge of the NSR. The shell thickness is taken to be ∼14% from the southwest edge, as the inner and outer boundaries of this part of the NSR shell are ∼87 pc and ∼101 pc from the nova, respectively. This possible compression front may indicate interaction of a bow shock with an earlier phase of the remnant's evolution, as seen with a similar feature in the KT Eri NSR, (Healy-Kalesh et al. 2024a). Additionally, there appears to be an interaction with a complex structure to the west (Fig. B.2) composed of many H II regions (Pellegrini et al. 2012).

Following Points et al. (2024), the H$\alpha$ and [S II] surface brightnesses of the bright northeast component of the NSR are $4.1 \times 10^{-17}$ erg cm$^{-2}$ s$^{-1}$ arcsec$^{-2}$ and $2.5 \times 10^{-17}$ erg cm$^{-2}$ s$^{-1}$ arcsec$^{-2}$, respectively. The H$\alpha$ and [S II] surface brightnesses of the bright southwest component are marginally fainter, radiating at $2.2 \times 10^{-17}$ erg cm$^{-2}$ s$^{-1}$ arcsec$^{-2}$ and $1.4 \times 10^{-17}$ erg cm$^{-2}$ s$^{-1}$ arcsec$^{-2}$, respectively.

### 3.1. NSR in radio data

As shown in Fig. 1, the H I data cube from the HI4PI survey (HI4PI Collaboration 2016) sliced at ∼294 km s$^{-1}$ and ∼314 km s$^{-1}$, reveals a correlated structure coincident with the H$\alpha$ shell. Specifically, the southwestern portion of the NSR shows a higher level of emission from in the ∼294 km s$^{-1}$ slice, while a possible shell boundary appears to the northeast in the ∼314 km s$^{-1}$ slice. A velocity distribution across the NSR, spanning 280 − 320 km s$^{-1}$ in declination and right ascension (see Fig. B.3 for the slits used) reveals an arc with a range of ∼20 km s$^{-1}$, as shown in Fig. B.4, possibly indicating an outer shell expansion velocity of ∼10 km s$^{-1}$. In MeerKAT radio data (Cotton et al., in prep.), there does not appear to be a corresponding structure, as shown in Fig. 1. By estimating the RMS noise level in the region of the NSR shell, we derive an upper limit of ∼30 μJy / beam.

### 3.2. Simple model of NSR evolution

To understand the evolutionary history of the NSR, we employed the hydrodynamical code `Morpheus` (Vaytet et al. 2007) following Healy-Kalesh et al. (2023, 2024a), to produce a simple model of the growth of such a remnant with a radius of ∼100 pc. For the eruption characteristics of LMCN 1971-08a, we utilised the data from (Bode et al. 2016), taking the recurrence period of the nova to be 38 years; the mass loss phase to be 10.4 days (equal to the $V$-band $t_3$ decline time); the ejecta velocity to be 4000 km s$^{-1}$; and the ejecta mass to be $1.4 \times 10^{-5}$ $M_\odot$.

To estimate the surrounding ISM density for the model, we took the H I data velocity cube from the HI4PI survey (HI4PI Collaboration 2016), converted the integrated intensity in the range of 280−320 km s$^{-1}$ into column density $N_H$ (using Eq. 2 from HI4PI Collaboration 2016), and found the average $N_H$ within 12′ of the nova (to incorporate the NSR and its surroundings). Assuming a depth of 5 kpc (estimated from the NSR's location in Fig. 9 of Subramanian & Subramaniam 2009) gives an ISM density of $6.68 \times 10^{-26}$ g cm$^{-3}$ (number density of $n = 0.04$ cm$^{-3}$).

With a nova system mimicking LMCN 1971-08a in a pre-populated ISM estimated for the local region, it would take $2.37 \times 10^6$ years over ∼62 400 eruptions to reach a radius of 100 pc, containing an evacuated cavity region ∼15 pc in radius. The NSR outer shell would have a mass of ∼4130 $M_\odot$ (made up almost exclusively of ISM) and an expansion velocity of

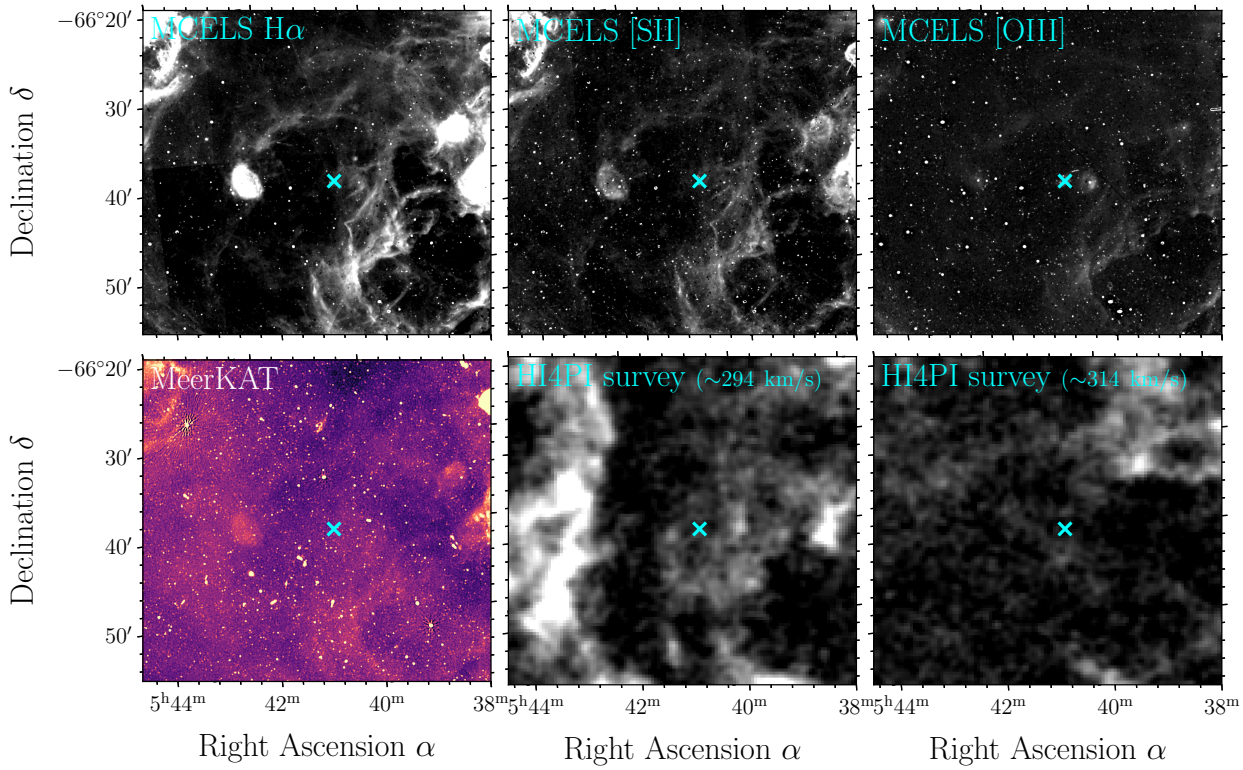


**Fig. 1.** Approximate 40 × 40 arcminute field of view showing the nova super-remnant around LMCN 1971-08a seen across different surveys and wavebands. The location of the nova is indicated with the cyan cross in each panel. The top row shows the surroundings of the nova in MCELS continuum-subtracted H$\alpha$, [S II] and [O III] data, with the NSR apparent in H$\alpha$ and [S II] but negligible in [O III]. The bright "stars" in the MCELS images are points of oversubtraction from saturated stars. The left panel on the bottom row showing MeerKAT data does not clearly reveal a corresponding structure. The middle and right panels in the bottom row show data cube slices at ~294 km s$^{-1}$ and ~314 km s$^{-1}$, respectively, from the HI4PI survey, with potential evidence for the same northeast (in the 314 km s$^{-1}$ panel) and southwest (in the 294 km s$^{-1}$ panel) components of the NSR seen in the optical.

~20 km s$^{-1}$, which is consistent with the expansion velocity derived from the H I position-velocity analysis from Sect. 3.1.

## 4. Discussion

### 4.1. Comparison to other NSRs

With a diameter of ~200 pc, the LMCN 1971-08a NSR is ~1.5 times larger than the NSR around M31N 2008-12a (major axis of 134 pc; Darnley et al. 2019) and a factor of ~4, 3, and 6.5 times larger than the NSRs associated with KT Eri (~50 pc; Shara et al. 2024b), T CrB (~30 pc; Shara et al. 2024c) and RS Oph (~70 pc; Shara et al. 2025), respectively. The projected morphology of the NSR is also more circular than the other NSRs, likely resulting from the system's inclination, and is most similar to the M31N 2008-12a NSR with more defined edges than the irregular morphology of the Galactic NSRs.

As with all other NSRs, this NSR is most prominent through its H$\alpha$ and [S II] emission. The H$\alpha$ surface brightnesses of the brightest component of the NSR (northeast part) is 4.1 × 10$^{-17}$ erg cm$^{-2}$ s$^{-1}$ arcsec$^{-2}$. Having an H$\alpha$ surface brightness comparable to the other NSRs – 4 × 10$^{-17}$ erg cm$^{-2}$ s$^{-1}$ arcsec$^{-2}$ for KT Eri (Shara et al. 2024b), ~6.6 × 10$^{-18}$ erg cm$^{-2}$ s$^{-1}$ arcsec$^{-2}$ for T CrB (Shara et al. 2024c), ~1.4 × 10$^{-17}$ erg cm$^{-2}$ s$^{-1}$ arcsec$^{-2}$ for RS Oph (Shara et al. 2025), and ~1 × 10$^{-16}$ erg cm$^{-2}$ s$^{-1}$ arcsec$^{-2}$ for M31N 2008-12a (based on integrated H$\alpha$ + [N II] flux; Darnley et al. 2019) – this NSR is intrinsically brighter than all others, supporting predictions that larger NSRs should be brighter (Healy-Kalesh et al. 2023). Moreover, the NSR shell is almost negligible in the [O III] narrowband filter (Fig. B.6) due to the lack of photoionisation across the structure, consistent with the findings of other NSRs (Darnley et al. 2019; Shara et al. 2024b,c, 2025). However, the southwest part does exhibit very faint [O III] emission coinciding with a higher [S II]/H$\alpha$ ratio.

The H I position-velocity analysis indicates a possible expansion velocity of the NSR outer edges of ~10 km s$^{-1}$. These velocities are consistent with those expansion velocities seen in other NSRs shells (Darnley et al. 2019; Shara et al. 2024b, 2025) and are in agreement with the range of NSR outer shell velocities predicted by modelling in this work and other studies (e.g.,Healy-Kalesh et al. 2023).

Both LMCN 1971-08a and another NSR-hosting nova KT Eri exhibit "several remarkable similarities" (Bode et al. 2016). Those authors suggested that both novae may belong to a class of RNe with WDs approximately 0.1–0.3 M$_\odot$ below the Chandrasekhar limit, but with very high mass transfer rates between eruptions. This similarity may indicate a potential correlation between these types of novae and the brightest NSRs, although this cannot be tested further until the sample of known NSRs increases.

### 4.2. Other origins

It is necessary to consider alternative origins of the visible shell encompassing LMCN 1971-08a, including it being a supernova remnant (SNR), a superbubble, a planetary nebula (PN), or an H II region. We therefore searched for sources within the NSR

(∼7′ radius) using SIMBAD (Wenger et al. 2000) and derived emission line ratios ([O III]/H$\alpha$, [S II]/H$\alpha$, and [O III]/[S II]; see Appendix A.3) for a consideration of these alternative scenarios.

While the structure is bright in H$\alpha$ and [S II], the low levels of [O III] emission (see Appendix A.3 and Fig. B.6) and lack of radio emission (see MeerKAT panel in Fig. 1) from the shell (both typical of SNR shock fronts), the absence of radio sources within the structure, the low expansion velocities inferred from H I data (see Sect. 3.1), and its size exceeding that of any SNR in the LMC (e.g., Zangrandi et al. 2024) together demonstrate that the discovered structure is not an SNR. The absence of strong [O III] emission (see Fig. B.6) and the size of the shell (LMC PNe are unresolved in MCELS data as they are arcsec-scale; e.g., Shaw et al. 2001) rule out a PN origin. There is one young stellar object (Whitney et al. 2008), one cluster of stars (Bica et al. 2008), and two associations of stars (Bica et al. 2008) within the shell. However, their classification does not specify whether they are OB associations (Bica et al. 2008), which could ionise the local ISM and create a bubble of this size (Wright 2020). Also, the structure is absent from the H II region catalogue by Pellegrini et al. (2012), arguing against it being an H II region or a superbubble. This is further supported by the lack of radio emission and the relatively high [S II]/H$\alpha$ ratio (see Fig. B.7).

### 4.3. Confirmation of recurrent nature

LMCN 1971-08a is deemed an RN on account of its spatial coincidence with the location of nova N LMC 1971b (Bode et al. 2016). Nevertheless, some scepticism has remained regarding its recurrent nature; for example, the entry for LMC 2009-02 (another identifier for LMCN 1971-08a) in Table 7 of Orio et al. (2021) is labelled as "perhaps" an RN, unlike other confirmed RNe in the LMC. Thus, the discovery of an NSR around this nova further supports its classification as an observationally defined RN, albeit from a different approach. In addition, owing to the existence of such an NSR, LMCN 1971-08a may have a much shorter recurrence period than the 38 years currently presumed and may therefore be observed in eruption much sooner than 2047.

## 5. Summary

In this Letter, we detailed the discovery of a nova super-remnant in the LMC, hosted by the recurrent nova LMCN 1971-08a. The structure is spatially coincident with the nova's location, spans ∼200 pc in diameter – making it the largest NSR found to date – and is visible in narrowband H$\alpha$ and [S II] emission indicative of shock-ionisation, but exhibits negligible [O III] emission. A corresponding structure is apparent in H I data. Adding to the growing collection of such NSRs, this is the first to be discovered in the LMC, the brightest NSR observed to date, and only the second extragalactic nova shell identified after the M31 NSR.

*Acknowledgements.* We thank the referee for feedback that improved our study. MS and FZ acknowledges support from the DFG through the grants SA 2131/13-2, SA 2131/14-2, and SA 2131/15-2. This work made use of the high performance computing facilities at Liverpool John Moores University, partly funded by LJMU's FET and by the Royal Society. This project used data obtained with the Dark Energy Camera (DECam), which was constructed by the Dark Energy Survey (DES) collaboration. Funding for the DES Projects has been provided by the DOE and NSF (USA), MISE (Spain), STFC (UK), HEFCE (UK), NCSA (UIUC), KICP (U. Chicago), CCAPP (Ohio State), MIFPA (Texas A&M), CNPQ, FAPERJ, FINEP (Brazil), MINECO (Spain), DFG (Germany) and the Collaborating Institutions in the Dark Energy Survey, which are Argonne Lab, UC Santa Cruz, University of Cambridge, CIEMAT-Madrid, University of Chicago, University College London, DES-Brazil Consortium, University of Edinburgh, ETH Zürich, Fermilab, University of Illinois, ICE (IEEC-CSIC), IFAE Barcelona, Lawrence Berkeley Lab, LMU München and the associated Excellence Cluster Universe, University of Michigan, NSF NOIRLab, University of Nottingham, Ohio State University, OzDES Membership Consortium, University of Pennsylvania, University of Portsmouth, SLAC National Lab, Stanford University, University of Sussex, and Texas A&M University. Based on observations at NSF Cerro Tololo Inter-American Observatory, NSF NOIRLab (NOIRLab Prop. ID 2018B-0908; PI: T. Puzia) and (NOIRLab Prop. ID 2021B-0060; PI: S. Points), which is managed by the Association of Universities for Research in Astronomy (AURA) under a cooperative agreement with the U.S. National Science Foundation. This research has made use of the SIMBAD database, operated at CDS, Strasbourg, France (see Wenger et al. 2000). This research has made use of the VizieR catalogue access tool, CDS, Strasbourg, France. The original description of the VizieR service was published in Ochsenbein et al. (2000).

## References

Bica, E., Bonatto, C., Dutra, C. M., & Santos, J. F. C. 2008, MNRAS, 389, 678
Bode, M. F., Darnley, M. J., Beardmore, A. P., et al. 2016, ApJ, 818, 145
Caldwell, N., Raymond, J. C., Long, K. S., & Lee, M. G. 2025, ApJ, 983, 150
Darnley, M. J., Hounsell, R., O'Brien, T. J., et al. 2019, Nature, 565, 460
Flaugher, B., Diehl, H. T., Honscheid, K., et al. 2015, AJ, 150, 150
Graham, J. A. 1971, IAU Circ., 2353, 1
Guerrero, M. A., Toalá, J. A., Medina, J. J., et al. 2013, A&A, 557, A121
Healy-Kalesh, M. 2024, in The Golden Age of Cataclysmic Variables and Related Objects - VI, 35
Healy-Kalesh, M. W., Darnley, M. J., Harvey, É. J., et al. 2023, MNRAS, 521, 3004
Healy-Kalesh, M. W., Darnley, M. J., Shara, M. M., et al. 2024a, MNRAS, 529, 236
Healy-Kalesh, M. W., Darnley, M. J., & Shara, M. M. 2024b, MNRAS, 528, 3531
Healy-Kalesh, M. W., Darnley, M. J., Harvey, É. J., & Newsam, A. M. 2024c, MNRAS, 529, L175
HI4PI Collaboration (Ben Bekhti, N., et al.) 2016, A&A, 594, A116
Hillman, Y., Prialnik, D., Kovetz, A., & Shara, M. M. 2016, ApJ, 819, 168
Kerp, J., Winkel, B., Ben Bekhti, N., Flöer, L., & Kalberla, P. M. W. 2011, Astron. Nachr., 332, 637
Lanzetta, K. M., Gromoll, S., Shara, M. M., et al. 2023, PASP, 135, 015002
Liller, W. 2009, IAU Circ., 9019, 1
McClure-Griffiths, N. M., Pisano, D. J., Calabretta, M. R., et al. 2009, ApJS, 181, 398
Jonas, J., & MeerKAT Team 2016, in MeerKAT Science: On the Pathway to the SKA, 1
O'Brien, T. J., Davis, R. J., Bode, M. F., Eyres, S. P. S., & Porter, J. M. 2001, Int. Astron. Union, 205, 260
Ochsenbein, F., Bauer, P., & Marcout, J. 2000, A&AS, 143, 23
Orio, M., Mason, E., Gallagher, J., & Abbott, T. 2009, ATel., 1930, 1
Orio, M., Dobrotka, A., Pinto, C., et al. 2021, MNRAS, 505, 3113
Peimbert, M., Peimbert, A., & Delgado-Inglada, G. 2017, PASP, 129, 082001
Pellegrini, E. W., Oey, M. S., Winkler, P. F., et al. 2012, ApJ, 755, 40
Pietrzyński, G., Graczyk, D., Gallenne, A., et al. 2019, Nature, 567, 200
Points, S. D., Long, K. S., Blair, W. P., et al. 2024, ApJ, 974, 70
Santamaría, E., Guerrero, M. A., Ramos-Larios, G., Toalá, J. A., & Sabin, L. 2025, MNRAS, 539, 246
Sasaki, M., Zangrandi, F., Filipović, M., et al. 2025, A&A, 693, L15
Shara, M. M., Lanzetta, K. M., Garland, J. T., et al. 2024a, MNRAS, 529, 212
Shara, M. M., Lanzetta, K. M., Garland, J. T., et al. 2024b, MNRAS, 529, 224
Shara, M. M., Lanzetta, K. M., Masegian, A., et al. 2024c, ApJ, 977, L48
Shara, M. M., Lanzetta, K. M., Masegian, A., et al. 2025, AJ, 170, 56
Shaw, R. A., Stanghellini, L., Mutchler, M., Balick, B., & Blades, J. C. 2001, ApJ, 548, 727
Smeaton, Z. J., Filipović, M. D., Alsaberi, R. Z. E., et al. 2025, Serbian. Astron. J., 210, 13
Smith, R. C., & Team, M. 1999, IAU Symp., 190, 28
Starrfield, S., Truran, J. W., Sparks, W. M., & Kutter, G. S. 1972, ApJ, 176, 169
Subramanian, S., & Subramaniam, A. 2009, A&A, 496, 399
Tosi, S., Dell'Agli, F., Kamath, D., et al. 2024, A&A, 688, A36
Vaytet, N. M. H., O'Brien, T. J., & Bode, M. F. 2007, ApJ, 665, 654
Wenger, M., Ochsenbein, F., Egret, D., et al. 2000, A&AS, 143, 9
Whelan, J., & Iben, I. Jr 1973, ApJ, 186, 1007
Whitney, B. A., Sewilo, M., Indebetouw, R., et al. 2008, AJ, 136, 18
Worters, H. L., Eyres, S. P. S., Bromage, G. E., & Osborne, J. P. 2007, MNRAS, 379, 1557
Wright, N. J. 2020, New Astron. Rev., 90, 101549
Yaron, O., Prialnik, D., Shara, M. M., & Kovetz, A. 2005, ApJ, 623, 398
Yew, M., Filipović, M. D., Stupar, M., et al. 2021, MNRAS, 500, 2336
Zangrandi, F., Jurk, K., Sasaki, M., et al. 2024, A&A, 692, A237

## Appendix A: Further remarks

### A.1. NSR missed in previous work

The LMC was surveyed in previous work (Healy-Kalesh et al. 2024b) through a targeted search around the four recurrent novae using the Faulkes Telescope South but no NSRs were uncovered. While 1.5 × 1.5 arcminute FOV images were provided in Healy-Kalesh et al. (2024b) around LMCN 1971-08a, the field of view of the Faulkes Telescope South facility used was 10.5 × 10.5 arcminutes (chosen to search the surroundings of the RNe for this reason by Healy-Kalesh et al. 2024b). As such, the region observed was large enough to capture a component of the NSR, however the relatively shorter exposure time of the observations (3 × 720s for H$\alpha$) and therefore fainter emission, in addition to (and more importantly) only a component of the NSR being captured, indicates why this structure was overlooked in the previous work. The FOV of the Faulkes Telescope South observation from Healy-Kalesh et al. (2024b) is shown in Fig. B.5. Now with knowledge of the gross structure of the NSR, the southwest shell edge can be made out when comparing with the DeMCELS image in Fig. B.5, as can the structure to the west of the nova's position.

### A.2. Surroundings of other LMC recurrent novae

The surroundings of all four RNe in the LMC were initially checked within the H$\alpha$ data of MCELS for signs of a NSR. While the NSR was discovered around LMCN 1971-08a, little is seen in the environments around LMCN 1968-12a, LMCN 1996 and YY Doradus.

### A.3. Comparison of line ratios with other possible structures

The ratios of emission lines can be used as diagnostic tools for helping to differentiate between different extended structures. As such, in Fig. B.6, we compare the [O III]/H$\alpha$ ratio for the nova super-remnant with the same ratio for three LMC supernova remnants, J0450-7050 (a.k.a. Veliki; Smeaton et al. 2025) and J0534-7033 and J0506-6541 (from Zangrandi et al. 2024); the LMC H II region, L77 DEM L45 (from Pellegrini et al. 2012); and the LMC planetary nebula, SMP LMC 80 (from Tosi et al. 2024), in order to differentiate the shell from other structures. We also provide similar comparative plots for the ratios [S II]/H$\alpha$ and [O III]/[S II] in Figs. B.7 and B.8, respectively.

The ratios were calculated for a number of apertures (with radii of 5″) along a slit passing through the structure (illustrated in Figs. B.6, B.7, and B.8). As the structures are different sizes, the length of the line (and therefore the number of apertures used) were scaled accordingly such that the ratios can be compared. The slit shown in Fig. B.6 is ∼1000″ long with 100 apertures for the nova super-remnant; ∼40″ long with 4 apertures for planetary nebula SMP LMC 80 (as PNe in the LMC are compact); ∼810″ long with 80 apertures for H II region L77 DEM L45; ∼400″ long with 40 apertures for SNR J0450-7050; ∼260″ long with 25 apertures for SNR J0534-7033; and ∼530″ long with 50 apertures for SNR J0506-6541. In the ratio plots of Figs. B.6, B.7, and B.8, the $x$-axes have been normalised.

**Supernova remnants** The emission line ratio [S II]/H$\alpha$ for supernova remnants is typically high (> 0.4 and see, e.g., Yew et al. 2021; Caldwell et al. 2025) as a result of enhanced ionisation and excitation of sulphur from radiative shocks (Zangrandi et al. 2024). In addition to this, SNRs also exhibit strong [O III] emission as a result of shock heating (Yew et al. 2021). While the nova super-remnant does exhibit a [S II]/H$\alpha$ ratio on par with the example supernova remnants (log([S II]/H$\alpha$) ∼ −0.1 and see Fig. B.7), there is a large difference in the [O III]/H$\alpha$ ratios for the NSR and the SNRs, with the NSR [O III] emission being much fainter (log([O III]/H$\alpha$) < −0.5) within the NE and SW component of the shell (between ∼0.05 − 0.13 and ∼0.86 − 0.95 on the $x$−axis of Fig. B.6).

**Planetary nebulae** Planetary nebulae have bright [O III] emission (Guerrero et al. 2013, and see the example PN in Fig. B.6) as a result of fast outflows shocking the surrounding low-density material (Guerrero et al. 2013) and weak [S II] emission (see, e.g., Caldwell et al. 2025). However, as can be seen in Fig. B.6, the nova super-remnant is faint in [O III] (with log([O III]/H$\alpha$) < −0.5 in the NE and SW component of the shell) and has moderate levels of [S II] emission (see Fig. B.7).

**H II regions** Typical H II regions have low [S II]/H$\alpha$ ratios as a result of the sulphur in such structures existing primarily as doubly-ionised sulphur (Yew et al. 2021) from the gas being photoionised (Zangrandi et al. 2024). As can be seen in Fig. B.7, the nova super-remnant has a higher [S II]/H$\alpha$ ratio across the shell than the ratio of a typical H II region. In addition, as illustrated with the example H II region in Fig. B.6, H II regions have high levels of [O III] due to photoionisation from hot central stars (Peimbert et al. 2017) however the discovered structure does not with log([O III]/H$\alpha$) < −0.5 for the NSR compared to log([O III]/H$\alpha$) > 0.2 for the H II region.

## Appendix B: Figures

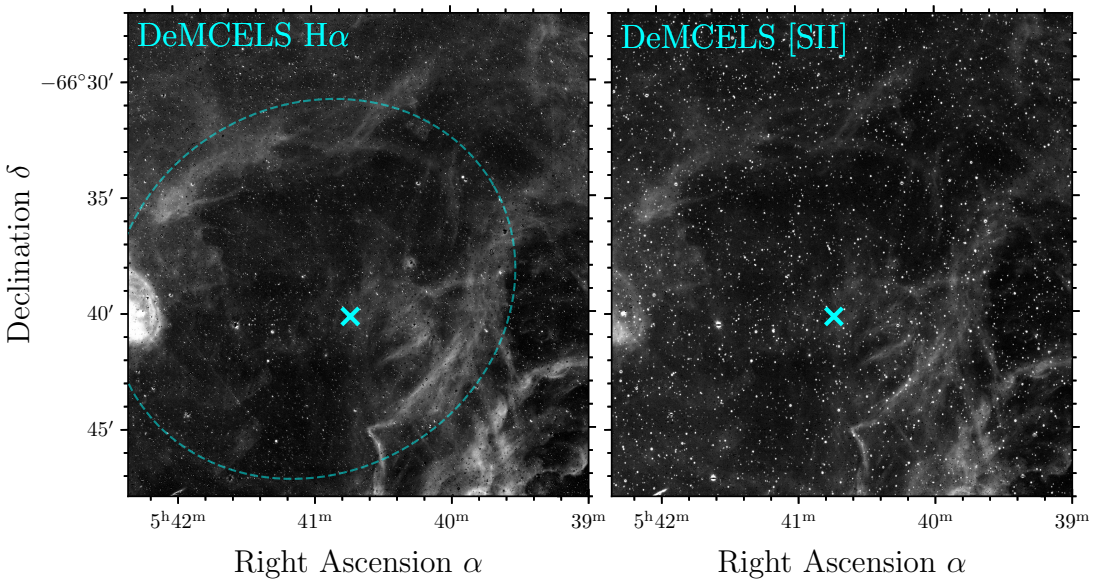


**Fig. B.1.** Left: DeMCELS continuum-subtracted H$\alpha$ image of the nova super-remnant surrounding the recurrent nova LMCN 1971-08a. The dashed ellipse is provided to approximately indicate the location of the NSR and its extent. The location of the nova is indicated by the cyan cross. Right: DeMCELS continuum-subtracted [S II] image of the same region. As with Fig. 1, the bright "stars" in the DeMCELS images are points of oversubtraction resulting from saturated stars in the R-band data used for continuum subtraction.

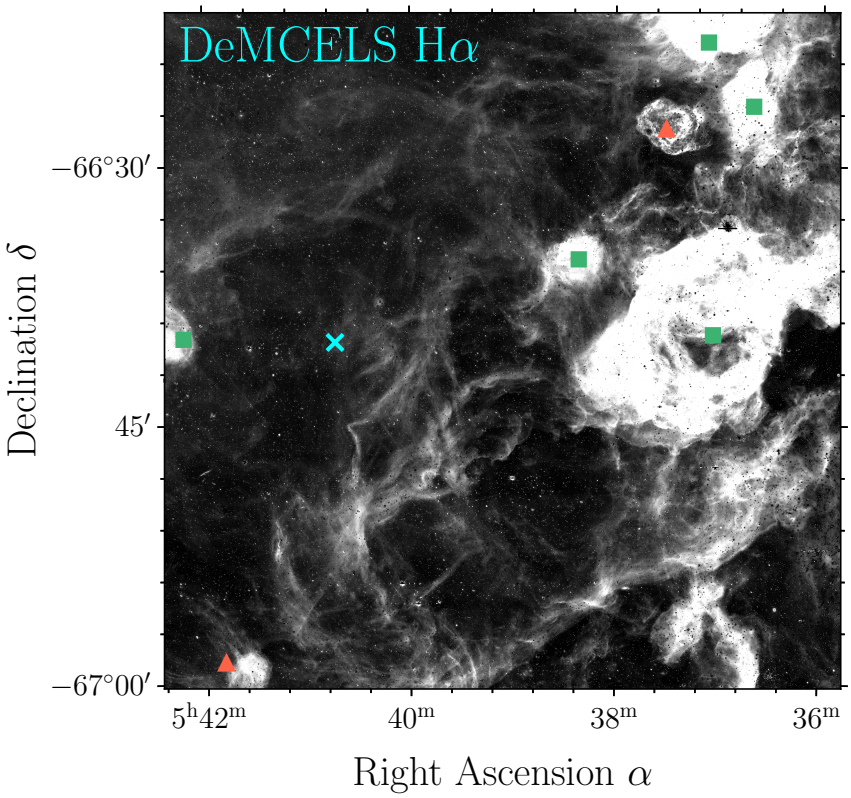


**Fig. B.2.** DeMCELS continuum-subtracted H$\alpha$ image with an approximately 39 × 39 arcminute field of view, showing the nova super-remnant surrounding LMCN 1971-08a and the extended environment including the multitude of H II regions to the west. The location of the nova is indicated by the cyan cross near the centre of the NSR shell. Other catalogued structures in the vicinity are labelled as follows: H II regions (green square) from Pellegrini et al. (2012) and SNRs (red triangles) from Zangrandi et al. (2024).

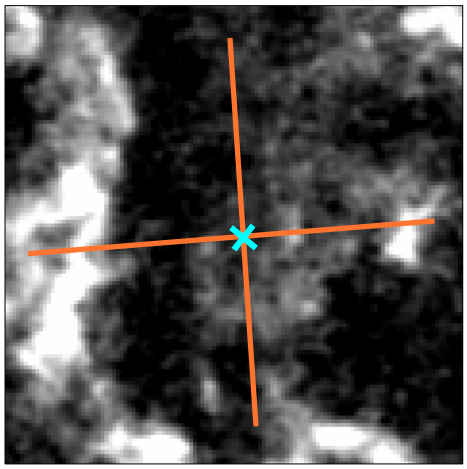

**Fig. B.3.** HI4PI survey image, as shown in Fig. 1 (at ~294 km s$^{-1}$), with the two slits used for the position-velocity analysis indicated with orange lines (one at constant right ascension and the other at constant declination). The location of the nova is marked with a cyan cross.

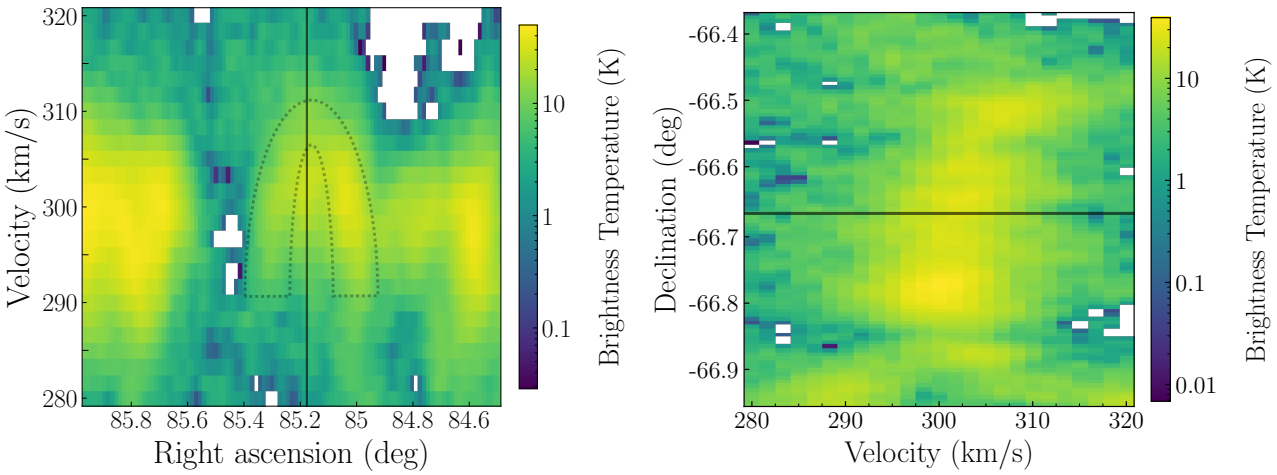


**Fig. B.4.** Parkes H I position-velocity diagrams around the position of the nova super-remnant. The location of LMCN 1971-08a is indicated by the dashed line. The arc ranging from ~290 – 310 km s$^{-1}$ is approximately outlined with a dashed line.

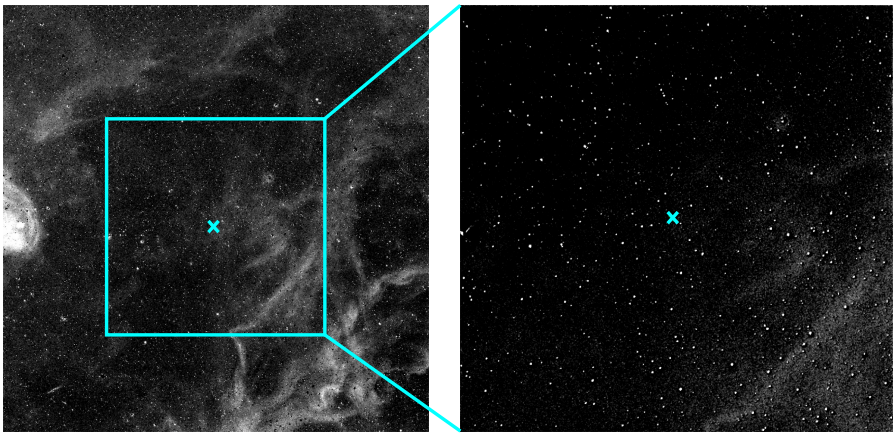

**Fig. B.5.** Faulkes Telescope South 10.5 × 10.5 arcminute field of view with the H$\alpha$ filter used in Healy-Kalesh et al. (2024b) overlaid onto the H$\alpha$ DeMCELS data (left panel). A part of the NSR was detected but overlooked in previous studies, mainly because the larger structure remained unidentified, and it was faint. The location of the nova is marked with the cyan cross.

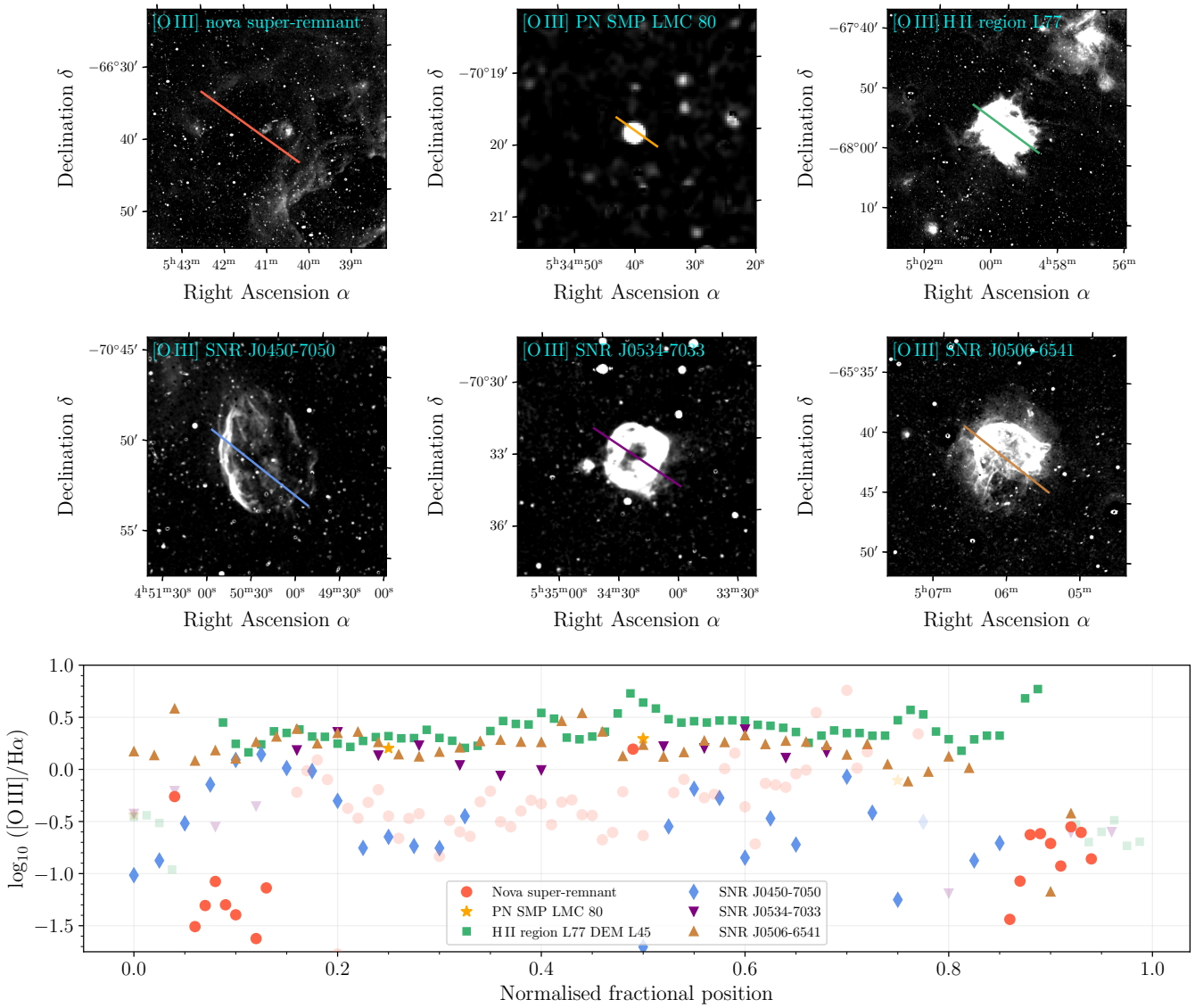


**Fig. B.6.** [O III]/H$\alpha$ ratios for the nova super-remnant, three supernova remnants, an H II region, and a planetary nebula. Top and middle rows: MCELS continuum-subtracted [O III] images of the six sources, each with a different field of view, as follows: ~33′ × 33′ for the NSR; ~3′ × 3′ for PN SMP LMC 80; ~40′ × 40′ for H II region L77 DEM L45; ~13′ × 13′ for SNR J0450-7050 (a.k.a. Veliki; Smeaton et al. 2025); ~10′ × 10′ for SNR J0534-7033; and ~20′ × 20′ for SNR J0506-6541. As detailed in Appendix A.3, slits with different lengths were placed across each structure (with different numbers of apertures) to derive ratios. These slits are shown in each panel. Bottom row: Comparison of the [O III]/H$\alpha$ ratios for the six sources across the length of the slit with the $x-$axis normalised to the length of the slit. The nova super-remnant has two distinct groupings of ratios (between ~0.05 − 0.13 and ~0.86 − 0.95) corresponding to the northeast and southwest shell with low [O III]/H$\alpha$ ratios. Two of the supernova remnants (J0534-7033 and J0506-6541) and the H II region have a high [O III]/H$\alpha$ ratio across their full extent, while the SNR J0450-7050 has a high [O III]/H$\alpha$ across the eastern edge. The [O III]/H$\alpha$ ratios from the two apertures across the PN are also high, as expected. The transparent points are from apertures with flux sums ≤ 0.

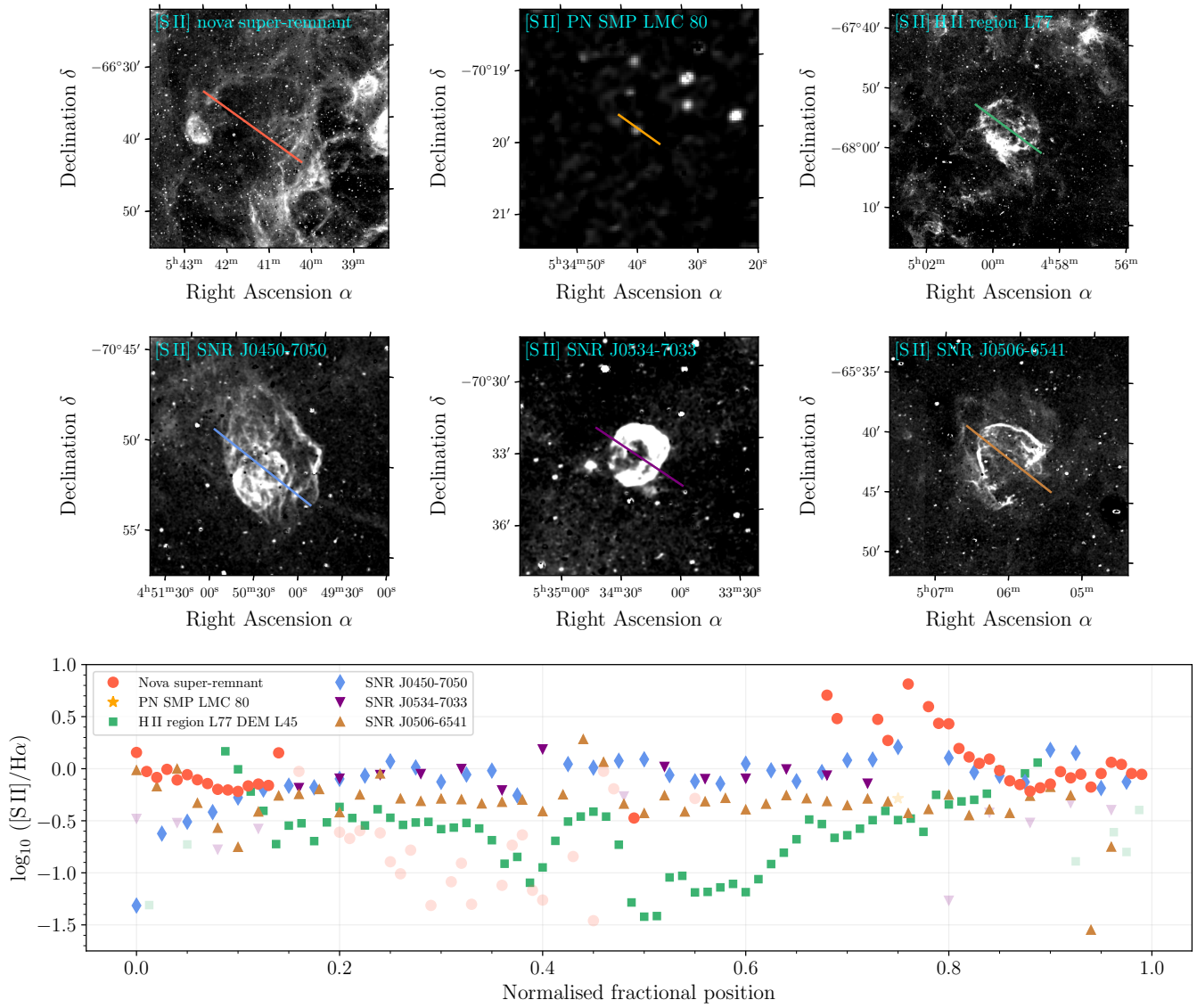


**Fig. B.7.** Same as Fig. B.6 but for the ratio [S II]/H$\alpha$. The top six panels show the MCELS continuum-subtracted [S II] images for the same six structures as in Fig. B.6. The bottom panel shows a comparison of the [S II]/H$\alpha$ ratio across the structures.

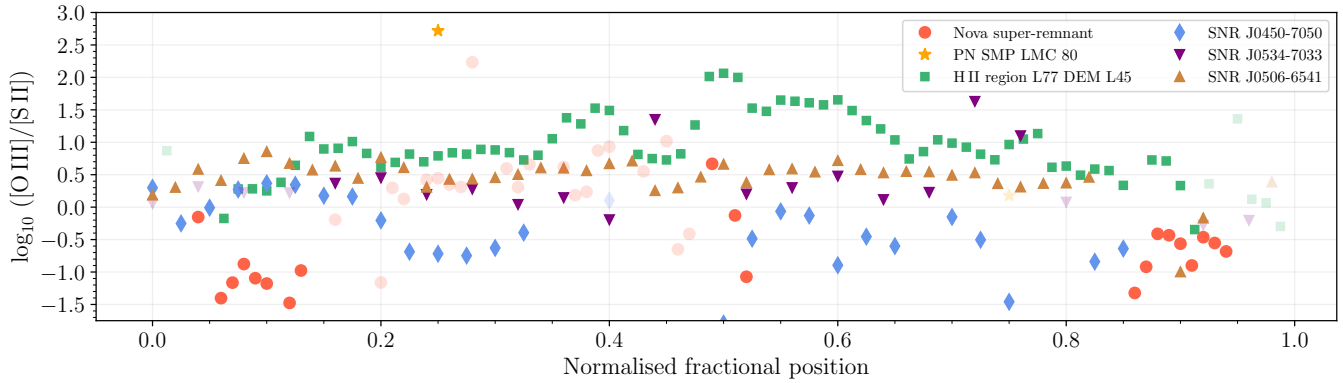


**Fig. B.8.** Comparison of the [O III]/[S II] ratio across the structure for the six sources shown in Fig. B.6. The line of apertures used is the same as in Fig. B.6. Note that the $y$-axis scale ranges from −1.75 to 3 here.